RSC Advances

PAPER

View Article Online
View Journal | View Issue

Cite this: *RSC Adv.*, 2019, **9**, 41561

Cu@Au(Ag)/Pt nanocomposite as peroxidase mimic and application of Cu@Au/Pt in colorimetric detection of glucose and L-cysteine†

Cuifeng Jiang,[a] Xiaoxiu Wei,[a] Shuai Bao,[a] Huajian Tu[a] and Wei Wang*[b]

Received 18th October 2019
Accepted 6th December 2019

DOI: 10.1039/c9ra08547e

rsc.li/rsc-advances

Nanomaterial-based artificial peroxidase has attracted extensive interests due to their distinct advantages over natural counterpart. Cu@Au/Pt and Cu@Ag/Pt nanocomposite with rambutan-like structure were prepared and discovered to function like peroxidase, which was illustrated by catalyzing the oxidation reaction of 3,3′,5,5′-tetramethylbenzidine (TMB) accompanied with a blue color change. Steady-state investigation indicates that the catalytic kinetics of Cu@Au/Pt and Cu@Ag/Pt all followed typical Michaelis–Menten behaviors and Cu@Au/Pt showed a strong affinity for H_2O_2, while Cu@Ag/Pt showed strong affinity for TMB. The color change and absorbance intensity strongly depend on the concentration of H_2O_2, thus the direct determination of H_2O_2 and indirect detection of glucose were demonstrated using Cu@Au/Pt with a detection limit of 1.5 μM and 6 μM, respectively. What is more important, the method was applied for detection of glucose in 50% fetal bovine serum with a detection limit of 80 μM, which is much lower than the lowest glucose content in blood for diabetes (7 mM). Moreover, the Cu@Au/Pt nanocomposite were also successfully applied for sensing L-cysteine because of the inhibition effect. Considering the good peroxidase-like activity and novel structure, Cu@Au(Ag)/Pt is expected to have a wide range of applications in bioassays and biocatalysis.

1. Introduction

Since the first report that Fe_3O_4 magnetic nanoparticles displayed peroxidase-like activity,[1] inorganic nanoparticle based artificial enzymes have been extensively studied because of their advantages over natural protein-based enzymes.[2] Compared to natural enzymes with chemical instability, high-cost and long-time preparation, nanoenzymes could offer unique advantages.[3,4] Among known nanoparticles, gold based nanoparticles are one of the most research-attractive materials for their catalytic activity.[5–7] Until now, bare AuNPs, chitosan–AuNPs,[8] cysteamine–AuNPs,[9] BSA–Au nanoclusters,[10] histidine–gold nanoclusters[11] have been found possessing intrinsic peroxidase-like activity. However, further improvement of catalytic ability of pure AuNPs was limited by the poor shape versatility and single ingredient. Therefore, extensive efforts have been made on the development of Au-based nanocomposite. For example, Au-loaded nanoporous ferric oxide nanocube,[12] Au@TiO_2 yolk–shell structure,[13] graphene/Au,[14] $ZnFe_2O_4$@Au,[15] Au@Ag nanorods,[16] Au@Pt nanorods,[17] Pt–Au NPs,[18] mercury-coated gold nanoparticles,[19] graphene supported Au–Pd–Fe_3O_4 (ref. 20) were reported to exhibit peroxidase catalytic ability. Inspired by the above work, we prepared Cu@Au(Ag)/Pt nanocomposite and explored its peroxidase-like activity.

As the primary source of energy for human body, glucose plays very important roles in physiological processes. However, disorder of glucose amount in blood will cause disease of diabetes. International Diabetes Federation reported, diabetes has become the fourth disease which leads to death in the world. Therefore, development of sensitive and selective approaches to determine concentration of glucose in blood obtains intensive attention. Different methods for glucose detection have been reported, such as colorimetric,[21–23] fluorescence,[24–26] surface enhanced Raman spectra (SERS),[27] dynamic light scattering[28] and electrochemical method.[29] Of these methods, colorimetric method attracted special attention due to its unique advantages like fast, simple and real-time monitoring.[30] Using peroxidase-like activity of nanomaterials to develop colorimetric assays for glucose detection was widely reported. These methods expand the application of artificial nanomaterials-based enzymes (nanozymes) and provide sensing diversity for glucose.[31–36] However, most of these methods display poor sensitivity or unfeasibility in complicated medium (*e.g.* serum). Hence, it is very meaningful to fabricate an analysis platform for glucose based on nanozymes with good sensitivity and applicability in more complicated medium. Moreover, the use of

[a]*School of Materials Science and Engineering, Yancheng Institute of Technology, Yancheng, Jiangsu, China, 224051*

[b]*School of Chemistry and Chemical Engineering, Yancheng Institute of Technology, Yancheng, Jiangsu, China, 224051. E-mail: wangw@ycit.edu.cn; ycitwangw@163.com*

† Electronic supplementary information (ESI) available. See DOI: 10.1039/c9ra08547e

Cu@Au/Pt nanocomposites as a peroxidase mimetic towards detection of glucose is novel and has not been reported yet.

Herein, Cu@Au/Pt or Cu@Ag/Pt nanocomposites were prepared by depositing Pt nanoparticles on the Cu@Au or Cu@Ag nanoparticles. The shape of nanocomposite was rambutan-like. Enzyme catalytic properties and steady-state kinetic assay of the nanocomposites were investigated. Special structure of rambutan-like with large surface area is helpful for the good catalytic activity. The R-Cu@Au/Pt NPs exhibited low detection limit for the sensing of hydrogen oxygen and glucose in serum. This study could provide important insight into the investigation of multicomponent nanostructure with excellent peroxidase mimic activity used as promising materials for analytical application.

2. Experimental

2.1 Materials and reagents

Hydrogen tetrachloroaurate trihydrate ($HAuCl_4 \cdot 3H_2O$), $NaBH_4$ and TMB were purchased from Sigma-Aldrich (Shanghai, China). Fetal bovine serum, glucose oxidase (GOX), H_2O_2, sodium citrate, 2,2′-azino-bis(3-ethylbenzthiazoline-6-sulfonic acid) (ABTS), $CuSO_4 \cdot 5H_2O$, L-ascorbic acid, glucose, lactose, maltose, sucrose, D-mannitol, L-cysteine and other kinds of amino acids were purchased from Sinopharm Chemical Reagent Co.,Ltd (Shanghai, China). K_2PtCl_6 was purchased from Aladdin (Shanghai, China). $AgNO_3$ was purchased from Energy Chemical (Shanghai, China). All the solutions were prepared with distilled water.

2.2 Instrumentations and characterizations

Photos of the samples were taken by using a Canon 80D digital camera. The micromorphology of as-prepared Cu@Au/Pt and Cu@Ag/Pt NCs were characterized by transmission electron microscopic (TEM) on a JEM-2011 with an accelerating voltage of 200 kV TEM. Ultraviolet-visible (UV-vis) extinction spectra were measured by using a Shimadzu UV-2600 spectrophotometer. The concentration of elements was determined using an inductively coupled plasma-optical emission spectroscopy (ICP-OES, PerkinElmer), in which the prepared Cu@Au/Pt solution were measured directly. X-ray photoelectron spectroscopy (XPS) measurements were performed with an ESCALAB 250Xi spectrometer. Zeta potential and dynamic light scattering (DLS) were estimated on a Malvern Zetasizer NANO ZS Grain Size using diluted nanoparticles in deionized water.

2.3 Experiment details

2.3.1 Preparation process

Cu@Au(Ag) nanoparticles. Preparation of Cu@Au nanoparticles (Cu@Au NPs) followed a literature procedure with minor modifications.[37] 50 μL of 0.1 M $CuSO_4$ and 50 μL of 0.1 M sodium citrate were added to 5 mL water. Then, 1 mL of 0.025 M freshly prepared $NaBH_4$ were added under vigorous stirring. 15 minutes later, 50 μL of 0.1 M $HAuCl_4 \cdot 3H_2O$ were added. After 20 min stirring, the solution were kept undisturbed at room temperature for 24 h. The obtained Cu@Au NPs were kept in 4 °C. When $HAuCl_4 \cdot 3H_2O$ was replaced with $AgNO_3$, Cu@Ag nanoparticles can be prepared.

Cu@Au(Ag)/Pt nanocomposite. 2 mL prepared Cu@Au NPs were added to 5 mL of 1.0 mM K_2PtCl_6 solution under stirring at 80 °C. Then, 5 mL of 5 mM L-ascorbic acid were added to the mixture dropwise. After stirring for 30 min. The nanocomposite were obtained. The concentration of Cu, Au and Pt elements in the final product were measured to be 5.1, 45.87 and 23.87 mg L^{-1} by ICP-OES. Cu@Ag/Pt nanocomposite can be prepared by using Cu@Ag NPs instead of Cu@Au NPs.

2.3.2 Verification of peroxidase-like activity and detection of hydrogen peroxide. The assays of the peroxidase activity were conducted in a 1.5 mL tube by sequentially adding 250 μL Cu@Au/Pt (or Cu@Ag/Pt), 100 μL 1.5 mM TMB, 100 μL 20 mM H_2O_2 and 100 μL 50 mM acetate buffer (pH = 3.8). After incubation at 30 °C for 10 min, the sample was estimated by absorption spectrophotometer using a 2 mm path length quartz cuvette. For detection of hydrogen oxygen, H_2O_2 with different concentration were added.

2.3.3 Steady-state kinetic assay. In order to obtain further insight into catalytic behavior of Cu@Au/Pt nanocomposites, the steady-state kinetic assays were carried out using 100 μL nanoparticles at the optimal condition (pH 3.8 and temperature 30 °C) by varying the concentration of H_2O_2 (0, 2, 4, 6, 8, 20, 30, 40, 50 mM) with a fixed concentration of TMB (1.5 mM), or varying concentration of TMB (0, 0.2, 0.4, 0.8, 2, 5, 10, 20, 30 mM) with fixed H_2O_2 concentration at 20 mM. The absorbance spectra of the mixture were recorded after 10 minutes incubation at 30 °C.

The kinetic parameters of catalytic activity were estimated by initial rate method on the basis of the Michaelis–Menten equation, $V_0 = V_{max}[S]/(K_m+[S])$, where V_0, V_{max} and $[S]$ represent the initial velocity of the reaction, the maximal rate of reaction and the substrate concentration, respectively. K_m is the Michaelis–Menten constant, indicating the affinity of the enzyme. Value of K_m is equivalent to the substrate concentration at which the rate of conversion is half of V_{max}.[38] V_{max} and K_m are also calculated from the Lineweaver–Burk double-reciprocal plot ($1/V_0$ *vs.* $1/[S]$). The absorbance signal were converted to concentration by the Beer–Lambert law ($A = \varepsilon bc$) where ε = 39 000 M^{-1} cm^{-1} at 652 nm for the oxidized TMB.[12]

2.3.4 Detection of glucose and L-cysteine. Detection of glucose was performed by three steps as following: different concentration of glucose with 20 μL of 5.0 mg mL^{-1} GOX were mixed in 10 mM phosphate buffer (pH = 7.4). The solution was incubated at 37 °C for 15 min and named solution (1).

35 μL prepared Cu@Au/Pt solution, 300 μL of 5 mM TMB, and 300 μL acetate buffer (pH = 3.8) were added to (1) solution, named (2) solution.

The mixture was incubated at 30 °C for 10 min for spectrophotometer detection. In control experiments, fructose, maltose and lactose with concentration of 5 mM was used instead of glucose.

The experiments were also performed by using serum as the media, in which different amounts of fetal bovine serum (with volume ratio of 10%, 30%, 50%) were added to (2) solution respectively. All the measurements were performed after incubation for 10 min.

For cysteine detection, 100 μL cysteine with different concentrations were added to mixture of 100 μL Cu@Au/Pt solution, 100 μL 1.5 mM TMB, 100 μL 20 mM H_2O_2 and 100 μL 50 mM acetate buffer. Then, the above solution was incubated at 30 °C for 10 min for further observation.

3. Results and discussion

Composite nanoparticles, such as Au-loaded nanoporous ferric oxide nanocube,[12] Au@TiO_2 yolk–shell structure,[13] γ-Fe_2O_3–SiO_2,[38] $Pt_{48}Pd_{52}$–Fe_3O_4 (ref. 39) were reported to exhibit peroxidase catalytic ability. Inspired by the above work, we prepared Cu@Au/Pt nanocomposite and explored its peroxidase-like activity. Cu@Au/Pt were prepared by using Cu@Au nanoparticles, K_2PtCl_6 and ascorbic acid as shown in Scheme 1. The shape of the nanocomposite was like rambutan, which has large surface areas. This nanocomposite with rambutan-like morphology showed good catalytic activity toward reaction of TMB and H_2O_2.

3.1 The characterization of the R-Cu@Au/Pt

The size and morphology of nanocomposite were analyzed by TEM images (Fig. 1). Fig. 1a indicated that Cu@Au NPs were nonspherical in shape and interconnected, in agreement with previous reported.[37] However, upon addition of K_2PtCl_6 and ascorbic acid, the interconnected nanoparticles growed to spherical nanoparticles with many thorns on the surface, which was like a rambutan. DLS results indicate the average hydrodynamic diameter of the nanocomposite was 130 nm, which is agreement with the TEM images. Energy dispersive spectrum results indicated existence of Au and Pt. XPS results also confirmed the formation of Cu@Au/Pt. Fig. S3(a–c)† depicts the XPS spectrum, which clearly indicates the presence of Cu, Au and Pt in the sample. Interestingly, morphology of Cu@Ag/Pt nanocomposite also showed as this rambutan-like structure with uniform size, while the Cu@Ag nanoparticles exhibited different shapes with wide size distribution (Fig. S1†). Therefore, formation of Pt is favorable for regular shapes. XPS spectrums (Fig. S3(d–f)†) of the nanocomposite showed the presence of Cu, Ag and Pt, indicating the formation of Cu@Ag/Pt. DLS results indicate the average hydrodynamic diameter of the Cu@Ag/Pt nanocomposite was 80 nm. Cu@Ag/Pd were prepared for comparison, and it also exhibited regular sphere shape. However, there is no thorns on the surface (Fig. S1†). Further reason is under investigation. Considering the large surface of this kind of structure, the nanocomposite perhaps hold potential application on catalysis, drug delivery, and so on. It has been reported ion migration into solution from surfaces containing Cu, Ag or Au element may happen, which resulted in higher corrosion resistance and biologically activity.[40] Therefore, the ion migration may be one reason for the good stability of Cu@Au/Pt and Cu@Ag/Pt nanocomposite, which can be stored for more than one month.

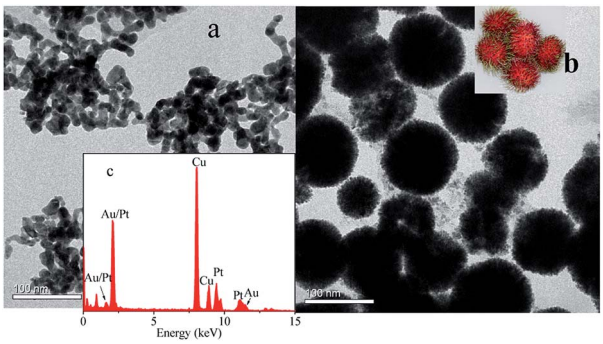

Fig. 1 (a) TEM images of Cu@Au NPs and (b) Cu@Au/Pt (inset is picture of rambutan) (c) EDS of Cu@Au/Pt.

3.2 The peroxidase-and oxidase-like activity of the Cu@Au/Pt nanocomposite

To demonstrate the peroxidase- and oxidase-like activity of the nanocomposite, the catalytic oxidation of the chromogenic substrate TMB in the presence and absence of H_2O_2 was tested. Fig. 2 shows the photographs and absorption spectra of the TMB solutions with different additions. As one can see, in the presence of H_2O_2, Cu@Au + TMB and Cu@Au/Pt + TMB system exhibited blue color, with deeper color in the Cu@Au/Pt + TMB system. Accordingly, a higher absorbance at 652 nm appeared in the Cu@Au/Pt + TMB + H_2O_2 system. Absorbance at 652 nm is a characteristic for oxidation of TMB. These results together indicate that Cu@Au/Pt can catalyze the oxidation of TMB in the

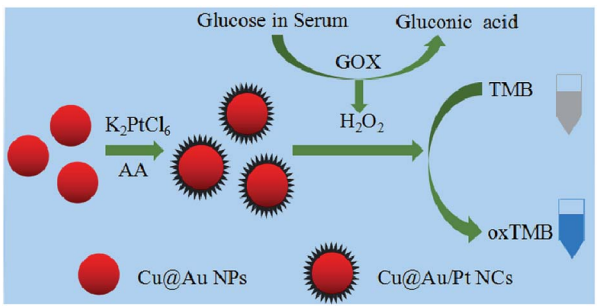

Scheme 1 Illustration of the preparation process for R-Cu@Au/Pt nanocomposites and sensing assay for glucose in serum.

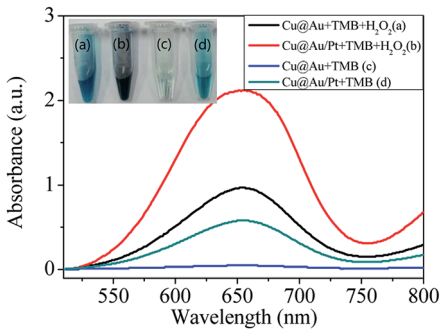

Fig. 2 Photo images and absorption spectra of (a) Cu@Au + TMB + H_2O_2 (b) Cu@Au/Pt + TMB + H_2O_2 (c) Cu@Au + TMB (d) Cu@Au/Pt + TMB (TMB: 5 mM, H_2O_2: 20 mM).

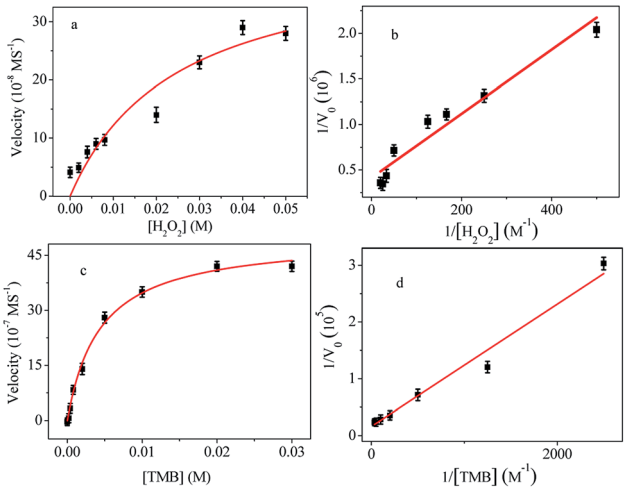

Fig. 3 Steady-state kinetic assays of the R-Cu@Au/Pt. (a) Varying H_2O_2 concentration with fixed TMB concentration (1.5 mM). (c) Varying TMB concentration with fixed H_2O_2 concentration (20 mM). (b and d) Lineweaver–Burk plots of the double reciprocal of the Michaelis–Menten equation.

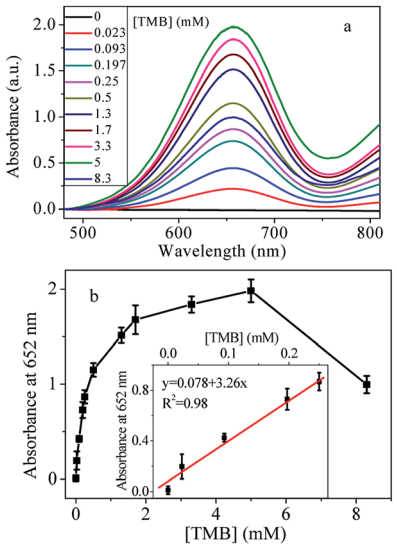

Fig. 4 (a) Absorption spectra of the sensing platform with increasing the concentration of TMB (H_2O_2: 20 mM). (b) The linear relationship between the relative absorption intensities and the concentration of TMB. Inset is the linear relationship in the low concentration. The error bars represent the standard deviation of three independent measurements.

presence of H_2O_2 and Cu@Au/Pt exhibits better peroxidase-like activity than Cu@Au. On the other hand, colorless of Cu@Au + TMB and lighter blue of Cu@Au/Pt + TMB demonstrate the better oxidase-like activity of Cu@Au/Pt. Such excellent performance of Cu@Au/Pt may be attributed to the small thorns of rambutan-like structure, which presents a large surface area. On the other hand, ion migration may be another reason responsible for the high catalytic ability.[40] ABTs are another chromogenic substrate. Experiments with ABTs as the substrate also exhibited peroxidase and oxidase-like activity for Cu@Au/Pt (Fig. S2†). Interestingly, the oxidase-like activity is stronger than peroxidase-like activity for Cu@Au/Pt. Zeta potential of the Cu@Au/Pt solution was measured to be −21.5 mV, indicating the negatively property of the solution. TMB has two amine groups, may show higher affinity towards negatively charged nanoparticles. In comparison, ABTs carries two sulfonic acid groups, likely yielding weaker affinity towards negatively charged nanoparticles.

3.3 Kinetics of the reaction

To investigate the catalytic activity of Cu@Au/Pt, the steady-state kinetic parameters were determined by altering the concentration of TMB and H_2O_2. Typical Michaelis–Menten curves were obtained for both H_2O_2 (Fig. 3a) and TMB (Fig. 3c). Kinetic parameters (K_m and V_m) were calculated from the Lineweaver–Burk double reciprocal plot (Fig. 3b and d) and compared with that of reported nanozymes (Table 1). Michaelis–Menten constant K_m, is an indicator of enzyme (or artificial enzyme) affinity towards its substrate, and a lower K_m indicates higher affinity between the enzyme and substrate.[12] Steady-state kinetic of R-Cu@Ag/Pt were also investigated and it follows Michaelis–Menten too (Fig. S4†). The apparent K_m value for R-Cu@Au/Pt with H_2O_2 was lower than that of Au-NPFe$_2$O$_3$NC and Fe$_3$O$_4$@Pt, indicating that the R-Cu@Au/Pt have stronger affinity with H_2O_2 in comparison to the previously reported composite nanoparticles, which is in agreement with the phenomenon that a lower H_2O_2 concentration was required to achieve the maximal catalytic activity for R-Cu@Au/Pt. This may be attributed to the shape of rambutan-like structure, which provides more "active sites" on the nanocomposite surface. However, Cu@Ag/Pt has lower K_m for TMB compared to Cu@Au/Pt.

Table 1 Comparison of the Michaelis–Menten constant (K_m) and maximum reaction rate (V_m) of Cu@Au/Pt with other catalysts

Catalyst	Substrate	K_m (mM)	V_m (M S^{-1})	Ref.
Au-NPFe$_2$O$_3$NC	TMB	0.0429	5.88×10^{-8}	8
	H_2O_2	138.5	4.77×10^{-8}	
Fe$_3$O$_4$@Pt	TMB	0.147	4.11×10^{-8}	41
	H_2O_2	702.6	7.14×10^{-7}	
Cu@Au/Pt	TMB	6.64 ± 0.24	$(6.14 \pm 0.2) \times 10^{-5}$	This work
	H_2O_2	8.54 ± 0.18	$(2.43 \pm 0.06) \times 10^{-6}$	
Cu@Ag/Pt	TMB	0.57 ± 0.014	$(4.02 \pm 0.12) \times 10^{-7}$	This work
	H_2O_2	8.5 ± 0.21	$(2.85 \pm 0.09) \times 10^{-7}$	

3.4 Optimization of the experimental conditions

It is well known that the substrate concentration, volume of catalyst, pH and temperature have a great impact on the peroxidase-like activity. In order to achieve optimal conditions, these parameters were evaluated. Firstly, the influence of TMB on the catalytic ability was investigated. As shown in Fig. 4, with increase the concentration of TMB, absorption peak increases significantly until 5 mM, after which the absorbance intensity decreases with increase of the TMB concentration. The highest absorbance signal was obtained at the concentration of 5 mM.

Catalytic reaction is related to the amount of the catalyst. Then, the peroxidase-like property could be influenced by the amount of Cu@Au/Pt nanocomposite. Therefore, the peroxidase-like activity was also investigated by changing the Cu@Au/Pt volume. Results in Fig. 5a showed there is almost no absorbance peak in the absence of Cu@Au/Pt nanoparticles. However, upon addition of 10 μL nanoparticles, a significant absorbance peak at 652 nm appeared, indicating the strong catalytic ability of nanocomposite. The absorption values at 652 nm increased with increase volume of Cu@Au/Pt. The absorbance intensity is linearly proportional to the volume of Cu@Au/Pt between 0-250 μL (Fig. 5b). The highest absorption value was obtained at 250 μL.

Reaction of TMB + H_2O_2 is sensitive to the experimental conditions. Thus, effect of pH and temperature were investigated to find the optimal experiment parameters. Firstly, a series of 50 mM acetate buffer with different pH values from 3.6 to 5.4 were prepared to explore the effect of pH on peroxidase-like activity of Cu@Au/Pt. Results in Fig. S5† indicate that peroxidase activity of the nanocomposite is sensitive to pH and the best result was obtained under pH of 3.8. Therefore, unless stated specially, pH of 3.8 is used in the following experiment.

Enzyme activity is usually temperature-dependent. Cu@Au/Pt nanocomposite, as a kind of artificial enzyme, its activity must be related to temperature. Therefore, the effect of temperature (20–90 °C) on nanocomposite's activity was investigated as well. The results in Fig. S6† indicated that the absorption at 652 nm decreased with the increase of temperature after 30 °C. It exhibited the highest catalytic activity when the temperature is 20 °C or 30 °C. Therefore, 30 °C is chosen in the following experiment. Importantly, the Cu@Au/Pt nanocomposite still shows catalytic activity even the temperature is raised up to 90 °C. This is better than natural enzyme of HRP, which would lose its activity once the temperature rises over 50 °C.[12] Clearly, wider activity temperature range could expand the application fields of nanocomposite.

3.5 Detection of H_2O_2 and glucose with Cu@Au/Pt nanocomposite

Considering the peroxidase-like property of Cu@Au/Pt, an analytical assay for detection of H_2O_2 can be designed. Thus, different concentration of H_2O_2 was added to Cu@Au/Pt + TMB system. As shown in Fig. 6a, in the absence of H_2O_2, the absorbance peak at 652 nm was very low. When 0.002 mM H_2O_2 was added, the absorbance increased obviously. With increase concentration of H_2O_2, the absorption increases dramatically until reached a plateau at 0.017 mM. The absorption almost remained unchanged when the concentration was higher than 0.017 mM, which means the TMB has been oxidized completely. On the basis of these results, a H_2O_2 concentration of 0.017 mM was chosen for further experiments. The absorption intensity at 652 nm is linearly proportional to the concentration of H_2O_2 in the range of 0–0.017 mM with the limit of detection (LOD) of 1.5 μM. Based on the proportional relationship, the Cu@Au/Pt

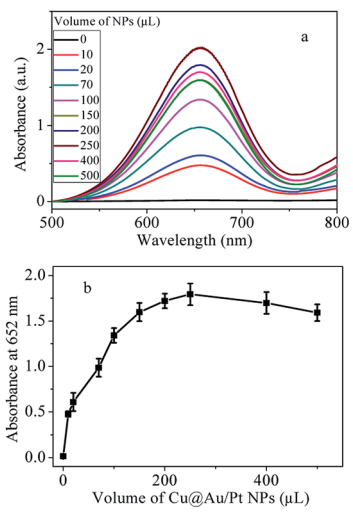

Fig. 5 (a) Absorption spectra of Cu@Au/Pt + TMB + H_2O_2 system with different volumes of nanoparticles. (b) The linear relationship between the relative absorption intensities and the volumes of nanoparticles (TMB: 5 mM, H_2O_2: 20 mM). The error bars represent the standard deviation of three independent measurements.

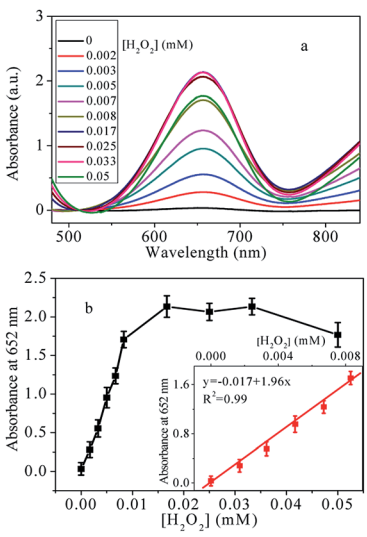

Fig. 6 (a) Absorption spectra of the sensing platform with increasing the concentration of H_2O_2. (b) The linear relationship between the relative absorption intensities and the concentration of H_2O_2. Inset is the linear relationship in the low concentration. The error bars represent the standard deviation of three independent measurements (TMB: 5 mM).

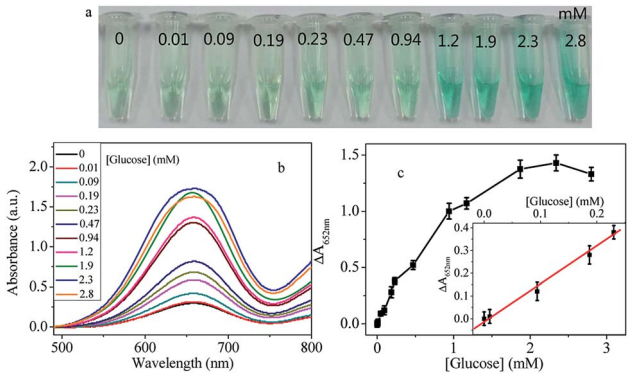

Fig. 7 (a) Colorimetric (b) absorption spectra of the sensing platform with increasing the concentration of glucose (c) the linear relationship between the Δ*A* and the concentration of glucose (TMB: 5 mM). Inset is the linear relationship in the low concentration. The error bars represent the standard deviation of three independent measurements.

could be used as a probe for detection of biological substance, which can generate H_2O_2 after reaction with their corresponding enzyme, such as glucose, cholesterol and uric acid. Especially, determination amount of glucose has attracted significant interest for the fast growing number of diabetes. Therefore, we chose glucose as the template substance to demonstrate the application of Cu@Au/Pt in analytical assays. Actually, this method can be expanded to detection of cholesterol, uric acid, and so on.

Under optimized experiment conditions, the analytical performance of this approach for glucose detection was evaluated. Results were presented in Fig. 7. It can be seen from Fig. 7a, upon addition of 0.01 mM glucose, remarkable deeper color was observed, which means the naked eye detection limit was estimated to be 0.01 mM. The oxidase-like property has certain influence on the determination of the naked eye detection limit. Even in the absence of glucose, lighter green color can be observed, which arises from the oxidase-like activity. The color of the solution became deeper gradually with the increased glucose. Meanwhile, the relative absorption intensities at 652 nm Δ*A* ($\Delta A = A - A_0$, where A and A_0 are absorption intensities in the presence and absence of glucose, respectively) with different concentration of glucose in Fig. 7c displayed that with increase concentration of glucose, the relative absorption intensities increased significantly, which is in agreement with the color change. The plot of the Δ*A* *versus* glucose concentration was plotted in Fig. 7c. Generally, the Δ*A* linearly correlated to glucose concentration until 1.9 mM glucose was added, where the Δ*A* almost kept unchanged with increase concentration of glucose. Therefore, the dynamic range is 0–1.9 mM. At low concentrations, the Δ*A* still demonstrates linearly toward glucose, with an equation of $y = 0.3 + 1.6x$ ($R^2 = 0.98$). The LOD for glucose, calculated as 3 times background divided by the slope, was estimated to be 6 μM. Comparison with other glucose detection methods, our proposed colorimetric assay exhibits lower or comparable LOD (Table 2). However, compared with other approaches, this method promises simplicity in operation, fast and high sensitivity.

Specificity is very important to assess the feasibility of an analytical approach. So a highly selective response towards glucose over other potentially interference is necessary. Analogues of glucose, including fructose, lactose, maltose, sucrose and D-mannitol were added respectively to test the specificity recognition to glucose. Results were presented in Fig. 8. It can be seen that the absorbance intensities of other substances were much lower than that of the glucose. The good selectivity could be due to the high specificity of glucose with GOX. Taken together, the designed platform provides a feasible detection method for glucose.

3.6 Analytical performance in serum

It is much important but difficult to detect glucose in blood serum because glucose exists in blood, which is a more complicated media than the buffer. Many sensing assays for glucose detection were performed in diluted serum media, such as fluorescence,[43] colorimetric[22,32] and upconversion luminescence.[44,45] Our platform based on peroxidase-like activity of Cu@Au/Pt was tested in the presence of fetal bovine serum with various volume ratios. The results in 10%, 30% and 50% serum are shown in Fig. S7† and summarized in Table S1.† The absorbance intensities in the serum were found to increase with increasing concentration of glucose (Fig. S7†). Results show that the absorbance is linearly proportional to the concentration of glucose. However, the detection limit is strongly dependent on the volume ratio of serum and increases when more serum was added. The LOD increases from 6 μM (0% serum) to 80 μM in 50% serum (Table S1†). Two reasons are responsible for the decreased sensitivity in serum. First, the serum itself exhibited some absorbance signal, which plays as the background noise and results in loss of sensitivity. On the other hand, fetal bovine serum is a complicated fluid containing a lot of proteins and other materials, which may prevent the affinity of TMB or H_2O_2 to nanoparticles, and cause a lower

Table 2 Comparison of the proposed approach with other reported colorimetric methods for the detection of glucose

Material	Method	LOD (μM)	Linear range (mM)	Ref.
CeO_2/nanotube-TiO_2	Colorimetric	6.1	0.01–0.5	42
Au@Ag nanorods	Colorimetric	39	0.05–20	16
γ-Fe_2O_3–SiO_2	Colorimetric	3.2	—	38
Au@TiO_2	Colorimetric	3.5	0–1	13
R-Cu@Au/Pt NPs	Colorimetric	6	0–1.9	This work

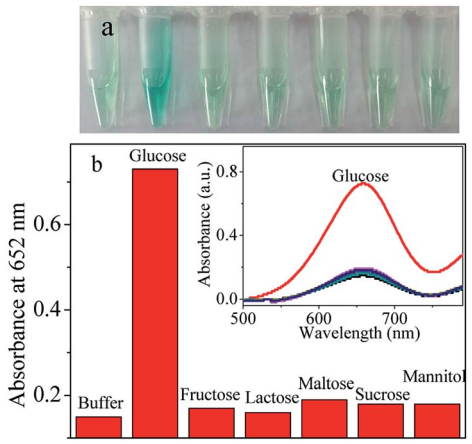

Fig. 8 (a) Colorimetric images and (b) absorbance intensity at 652 nm of the sensing assay in the presence of buffer, glucose, fructose, lactose, maltose, sucrose and D-mannitol (all the concentration was 0.5 mM. Inset is the corresponding UV-vis spectra) (TMB: 5 mM, H_2O_2: 20 mM).

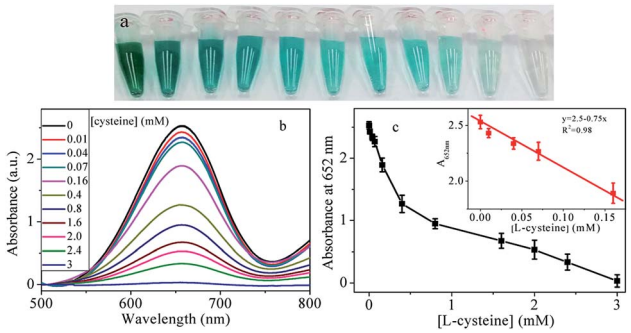

Fig. 9 (a) Colorimetric (b) absorption spectra of the sensing platform with increasing the concentration of L-cysteine (c) the linear relationship between the absorption intensities and the concentration of L-cysteine. Inset is the linear relationship in the low concentration. The error bars represent the standard deviation of three independent measurements.

sensitivity in comparison to that in the buffer solution.[46] These results revealed that the platform was practicable for detection of glucose in serum.

Literature reported L-cysteine could inhibit the peroxidase-like activity of nanoparticles through interaction of metal atoms in the surface of nanoparticles with –SH of cysteine.[47,48] Therefore, we investigated the possibility for the detection of L-cysteine using Cu@Au/Pt nanocomposite. Interestingly, when cysteine was added to the mixture of Cu@Au/Pt + TMB + H_2O_2, the color changed from blue to colorless and the absorbance at 652 nm decreased significantly, indicating that addition of cysteine inhibited the oxidation of TMB. Based on the phenomenon, we developed a colorimetric method for the detection of cysteine, which plays an important rule in many physiological processes. The standard cysteine response under optimal conditions is displayed in Fig. 9. It can be seen that the color became lighter (Fig. 9a) and absorbance decreased (Fig. 9b) with increase concentration of cysteine. The linear range is 0–0.4 mM and 0.4–3 mM with a detection limit of 4 μM. The assay also showed good selectivity towards cysteine among other amino acids (Fig. S8†). In order to detect the practicability, recovery experiments in tap water were conducted. Aliquots (100 μL) of tap water were spiked with standard cysteine solution with different concentrations. A certain volume of spiked sample were then mixed with Cu@Au/Pt, TMB and H_2O_2 in acetate buffer to a final volume of 500 μL for further measurement. As shown in Table S2,† the recovery lies in the range of 98–116%, which is in the acceptance range.

4. Conclusions

In summary, Cu@Au/Pt and Cu@Ag/Pt nanocomposite developed in this work can be used as peroxidase-like enzyme. Benefited from the large surface area of rambutan-like structure, the prepared nanocomposite exhibited remarkably catalytic activity. The optimum catalytic condition is pH 3.8 and temperature at 30 °C or 20 °C. On the basis of the catalytic property of the Cu@Au/Pt, simple and easy colorimetric detection technique was developed towards H_2O_2, glucose and cysteine with excellent sensitivity and selectivity. The results with LOD of 80 μM in 50% serum demonstrated the feasibility of the approach for detecting glucose in sophisticated biological environment. Another advantage of this sensing assay using Cu@Au/Pt is simple in operation, fast and sensitivity. This study is anticipated to promote the development of trimetallic nanocomposite for many biosensing and for potential applications in the field of biotechnology.

Conflicts of interest

There are no conflicts to declare.

Acknowledgements

This work was supported by the National Natural Science Foundation of China (Grant No. 21605128, 21876144, 21575123), the Initial Scientific Research Foundation of Yancheng Institute of Technology (No. xj201530).

References

1 L. Gao, J. Zhuang, L. Nie, J. Zhang, Y. Zhang, N. Gu, T. Wang, J. Feng, D. Yang, S. Perrett and X. Yan, *Nat. Nanotechnol.*, 2007, **2**(9), 577–583.
2 M. Nasir, M. H. Nawaz, U. Latif, M. Yaqub, A. Hayat and A. Rahim, *Microchim. Acta*, 2016, **184**(2), 323–342.
3 H. Wei and E. Wang, *Chem. Soc. Rev.*, 2013, **42**(14), 6060–6093.
4 L. Yan, H. Ren, Y. Guo, G. Wang, C. Liu, Y. Wang, X. Liu, L. Zeng and A. Liu, *Talanta*, 2019, **201**, 406–412.
5 Z. Zhang, Z. Chen and L. Chen, *Langmuir*, 2015, **31**(33), 9253–9259.
6 J. Feng, P. Huang, S. Shi, K. Y. Deng and F. Y. Wu, *Anal. Chim. Acta*, 2017, **967**, 64–69.

7 S. Wang, Z. Chen, J. Choo and L. Chen, *Anal. Bioanal. Chem.*, 2016, **408**(4), 1015–1022.
8 C. Jiang, J. Zhu, L. Zhao, J. Luo, J. Wang and Y. Sun, *RSC Adv.*, 2017, **7**, 44463–44469.
9 D. Zhao, C. Chen, L. Lu, F. Yang and X. Yang, *Sens. Actuators, B*, 2015, **215**, 437–444.
10 Y. Chang, Z. Zhang, J. Hao, W. Yang and J. Tang, *Sens. Actuators, B*, 2016, **232**, 692–697.
11 Y. Liu, D. Ding, Y. Zhen and R. Guo, *Biosens. Bioelectron.*, 2017, **92**, 140–146.
12 M. K. Masud, S. Yadav, M. N. Islam, N. T. Nguyen, C. Salomon, R. Kline, H. R. Alamri, Z. A. Alothman, Y. Yamauchi, M. S. A. Hossain and M. J. A. Shiddiky, *Anal. Chem.*, 2017, **89**(20), 11005–11013.
13 X. Peng, G. Wan, L. Wu, M. Zeng, S. Lin and G. Wang, *Sens. Actuators, B*, 2018, **257**, 166–177.
14 C. Chen, N. Li, J. Lan, X. Ji and Z. He, *Anal. Chim. Acta*, 2016, **902**, 154–159.
15 L. Shen, C. Chu, C. Ma, H. Yang, S. Ge, J. Yu, M. Yan and X. Song, *Sens. Actuators, B*, 2014, **201**, 196–203.
16 L. Han, C. Li, T. Zhang, Q. Lang and A. Liu, *ACS Appl. Mater. Interfaces*, 2015, **7**(26), 14463–14470.
17 J. Liu, X. Hu, S. Hou, T. Wen, W. Liu, X. Zhu, J.-J. Yin and X. Wu, *Sens. Actuators, B*, 2012, **166–167**, 708–714.
18 T. Jiang, Y. Song, T. Wei, H. Li, D. Du, M. J. Zhu and Y. Lin, *Biosens. Bioelectron.*, 2016, **77**, 687–694.
19 X.-J. Li, Y.-S. Wang, S.-Y. Yang, X. Tang, L. Liu, B. Zhou, X.-F. Wang, Y.-F. Zhu, Y.-Q. Huang and S.-Z. He, *Microchim. Acta*, 2016, **183**(7), 2123–2129.
20 J. Zhang, J. Ma, X. Fan, W. Peng, G. Zhang, F. Zhang and Y. Li, *Catal. Commun.*, 2017, **89**, 148–151.
21 N. Lu, M. Zhang, L. Ding, J. Zheng, C. Zeng, Y. Wen, G. Liu, A. Aldahlbahi, J. Shi, S. Song, X. Zuo and L. Wang, *Nanoscale*, 2017, **9**(13), 4508–4515.
22 Y. Xia, J. Ye, K. Tan, J. Wang and G. Yang, *Anal. Chem.*, 2013, **85**(13), 6241–6247.
23 J. Chen, Q. Chen, J. Chen and H. Qiu, *Microchim. Acta*, 2016, **183**(12), 3191–3199.
24 W. Na, H. Liu, M. Wang and X. Su, *Microchim. Acta*, 2017, **184**(5), 1463–1470.
25 S. K. Vaishanav, J. Korram, R. Nagwanshi, K. K. Ghosh and M. L. Satnami, *Sens. Actuators, B*, 2017, **245**, 196–204.
26 F. Tang, C. Wang, X. Wang and L. Li, *ACS Appl. Mater. Interfaces*, 2015, **7**(45), 25077–25083.
27 Q. Chen, Y. Fu, W. Zhang, S. Ye, H. Zhang, F. Xie, L. Gong, Z. Wei, H. Jin and J. Chen, *Talanta*, 2017, **165**, 516–521.
28 X. Miao, L. Ling and X. Shuai, *Biosens. Bioelectron.*, 2013, **41**, 880–883.
29 Y. Su, B. Luo and J. Z. Zhang, *Anal. Chem.*, 2016, **88**(3), 1617–1624.
30 M. S. Steiner, A. Duerkop and O. S. Wolfbeis, *Chem. Soc. Rev.*, 2011, **40**(9), 4805–4839.
31 A. Samanta, B. B. Dhar and R. N. Devi, *New J. Chem.*, 2012, **36**(12), 2625.
32 L. Jin, Z. Meng, Y. Zhang, S. Cai, Z. Zhang, C. Li, L. Shang and Y. Shen, *ACS Appl. Mater. Interfaces*, 2017, **9**(11), 10027–10033.
33 X. Jiang, C. Sun, Y. Guo, G. Nie and L. Xu, *Biosens. Bioelectron.*, 2015, **64**, 165–170.
34 Z. Zhang, Z. Chen, F. Cheng, Y. Zhang and L. Chen, *Biosens. Bioelectron.*, 2017, **89**(Pt 2), 932–936.
35 J. Yu, D. Ma, L. Mei, Q. Gao, W. Yin, X. Zhang, L. Yan, Z. Gu, X. Ma and Y. Zhao, *J. Mater. Chem. B*, 2018, **6**(3), 487–498.
36 H. Ren, L. Yan, M. Liu, Y. Wang, X. Liu, C. Liu, K. Liu, L. Zeng and A. Liu, *Sens. Actuators, B*, 2019, **296**, 126517.
37 T. Lou, H. Qiang and Z. Chen, *Talanta*, 2017, **163**, 132–139.
38 C. Lu, X. Liu, Y. Li, F. Yu, L. Tang, Y. Hu and Y. Ying, *ACS Appl. Mater. Interfaces*, 2015, **7**(28), 15395–15402.
39 X. Sun, S. Guo, C. S. Chung, W. Zhu and S. Sun, *Adv. Mater.*, 2013, **25**(1), 132–136.
40 D. Wojcieszak, M. Mazur, M. Kalisz and M. Grobelny, *Mater. Sci. Eng., C*, 2017, **71**, 1115–1121.
41 M. Ma, J. Xie, Y. Zhang, Z. Chen and N. Gu, *Mater. Lett.*, 2013, **105**, 36–39.
42 H. Zhao, Y. Dong, P. Jiang, G. Wang and J. Zhang, *ACS Appl. Mater. Interfaces*, 2015, **7**(12), 6451–6461.
43 C. Zong, M. Wang, B. Li, X. Liu, W. Zhao, Q. Zhang, A. L. a. and Y. Yu, *RSC Adv.*, 2017, **7**, 26559–26565.
44 H. Chen, A. Fang, L. He, Y. Zhang and S. Yao, *Talanta*, 2017, **164**, 580–587.
45 J. Liu, L. Lu, A. Li, J. Tang, S. Wang, S. Xu and L. Wang, *Biosens. Bioelectron.*, 2015, **68**, 204–209.
46 C. Jiang, T. Zhao, S. Li, N. Gao and Q. H. Xu, *ACS Appl. Mater. Interfaces*, 2013, **5**(21), 10853–10857.
47 M. Chi, Y. Zhu, L. Jing, C. Wang and X. Lu, *Anal. Chim. Acta*, 2018, **1035**, 146–153.
48 M. Singh, P. Weerathunge, P. D. Liyanage, E. Mayes, R. Ramanathan and V. Bansal, *Langmuir*, 2017, **33**(38), 10006–10015.